

---

**COMEDI**

**Ye Wu**

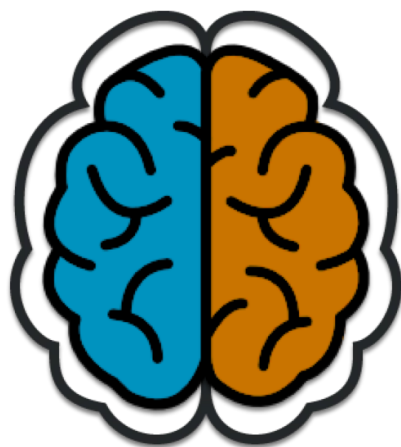
**Oct 12, 2021**



**INSTALL**

<b>1</b>	<b>Aims</b>	<b>3</b>
<b>2</b>	<b>Features</b>	<b>5</b>
<b>3</b>	<b>Table of Contents</b>	<b>7</b>
	<b>Bibliography</b>	<b>27</b>







**AIMS**

- **COMEDI** is a Matlab library for computational analysis of neuroscience.
- **COMEDI** aims to construct a free, open-source, and cross-platform one-stop project for computational neuroscience.





## FEATURES

- **COMEDI** provides a uniform I/O interface for most of the formats.
- **COMEDI** provides a unique API to call third-party software (e.g., FSL, MRtrix3, Dipy).
- **COMEDI** follows the BIDS style for data analysis.
- **COMEDI** provides the implements with multiple cores of a CPU, as well GPU.
- **COMEDI** provides the command line interface, an essential requirement to write scripts for processing big data in computer grids.
- **COMEDI** supports for easy and high quality visualizations with D3.js.

---

**Note:** We provides the [latest](#) source, the [released](#) source, and the [precompiled](#) binaries

---

**Warning:** This manual is showcasing the very basic tools of COMEDI. It is far from complete, but it's a start! Any feedback is always welcome...

Use of the **COMEDI** software package in published works should be accompanied by the following citations:

1. Wu, Y., Ahmad, S., Huynh, K.M., Liu, S., Thung, KH., Lin, W., P.-T. Yap, 2021. An Automated Processing Pipeline for Diffusion MRI in the Baby Connectome Project, ISMRM, May 15-20, 2021.

---

**Tip:** Make sure to use the version of this documentation that matches your version of this software. You can select the version on the lower left of this page.

---



## TABLE OF CONTENTS

### 3.1 Installation of COMEDI

#### 3.1.1 Precompiled binaries

##### *Before of installing*

Standalone version of COMEDI are available for Windows, Linux & Mac OS (only for 64 bit OS). With the standalone executable, there is no need have Matlab installed.

**It is recommended to install COMEDI on a computer with high-performance specs:**

1. multi-core CPU
2. RAM > 16 GB
3. dedicated graphics cards / GPU

If you already tried to run the executable ‘COMEDI’ before having read this part of the manual, you may have encountered the error message.

The standalone version of COMEDI is currently being developed in Matlab R2021b. The executable, ‘COMEDI’, only works after you installed the Matlab Common Runtime (MCR) libs of that Matlab version – you can download the one your OS of interest here:

##### *Download and install*

You can download the precompiled binaries from

To install the MCR libs file, simply follow the instructions. Note that MCR libraries from other Matlab versions are probably not compatible with these standalone versions of COMEDI. Again, note that you do NOT need a Matlab license to run COMEDI! For Linux/Mac, if you choose an installation directory for the MCR that is different from the default one, you need to use this path in the “run\_COMEDI.sh” as well

### 3.1.2 Release/Preview source

1. Clone the COMEDI repository:

```
$ git clone https://github.com/diffusionmri/COMEDI.git
```

or download the released COMEDI:

```
$ wget https://github.com/diffusionmri/COMEDI/archive/refs/tags/v1.0.zip
```

1. Configure the COMEDI install in Matlab:

```
>> cmdInstall
```

1. Keeping COMEDI up to date

You can update your installation at any time by opening at Matlab in the COMEDI folder, and typing:

```
>> cmdUpdate
```

If this doesn't work immediately, it may be that you need to re-setup the configure script:

```
>> cmdInstall
```

### 3.1.3 HPC cluster

These instructions outline a few issues specific to high-performance computing (HPC) systems.

Without more specifics! With HPC cluster, it is recommended to add a few lines of code in your job submission, for example

```
$ export SLURM_JOBTMP=/path/to/tmp/folder
$ export MATLAB_PREFDIR=$(mktemp -d $SLURM_JOBTMP/matlab-XXXX)
$ echo "Hostname: $(hostname)"
$ matlab -nodesktop -nosplash -nodisplay -r "yourfunction();exit;"
```

## 3.2 Computational Medical File (CMF)

### 3.2.1 Image format handling in *COMEDI*

*COMEDI* provides a flexible data input/output back-end in the shared library, which is used across all applications. This means that all applications in *COMEDI* can read or write images in all the supported formats - there is no need to explicitly convert the data to a given format prior to processing. Importantly, *COMEDI* uniquely uses an in-house designed *Computational Medical File (CMF) Format* for all the supportable data formats.

However, some specialized applications may expect additional information to be present in the input image. The *COMEDI* .cmf formats with class {cmdata} are both capable of storing such additional information data in their header, and will hence always be supported for such applications. Most image formats however cannot carry additional information in their header (or at least, not easily) - this is in fact one of the main motivations for the development of the *COMEDI* image formats. In such cases, it would be necessary to use *COMEDI* format images. Alternatively, it may be necessary to provide the additional information using command-line arguments.

## Coordinate system

All *COMEDI* applications will consistently use the same coordinate system, which is identical to the [NIFTI](#) standard.

## Multi-file numbered image support

It is possible to access a numbered series of images as a single multi-dimensional dataset, using a syntax specific to *COMEDI*. For example:

```
>> cminfo('MRI-volume-*.nii.gz')
```

will collate all images that match the pattern `MRI-volume-<number>.nii.gz`, sort them in ascending numerical order, and access them as a single dataset with dimensionality one larger than that contained in the images. In other words, assuming there are 10 `MRI-volume-0.nii.gz` to `MRI-volume-9.nii.gz`, and each volume is a 3D image, the result will be a 4D dataset with 10 volumes.

Note that this isn't limited to one level of numbering:

```
>> cmconvert('MRI-volume-*-*.nii.gz', 'MRI-volume.cmf')
```

will collate all images that match the `MRI-volume-*-*.nii.gz` pattern and generate a single dataset with dimensionality two larger than its constituents.

## Data types

*COMEDI* applications can read and write data in any of the common data types. Many *COMEDI* commands also support the `datatype` option to specify the data type for the output image. For example:

```
>> cmconvert('MRI-volume-*-*.nii.gz', 'MRI-volume.cmf', datatype='uint16') ;
```

**Note:** Not all image formats support all possible datatypes. The *COMEDI* image file formats are designed to handle all of the possibilities listed below, while other image formats may only support a subset. When a data type is requested that isn't supported by the image format, a hopefully suitable alternative data type will be used instead.

Below is a list of the supported data types and their specifiers for use on the command-line. Note that *COMEDI* is not sensitive to the case of the specifier: `uint16le` will work just as well as `UInt16LE`.

Specifier	Description
<code>double</code>	Double-precision arrays
<code>single</code>	Single-precision arrays
<code>int8</code>	8-bit signed integer arrays
<code>int16</code>	16-bit signed integer arrays
<code>int32</code>	32-bit signed integer arrays
<code>int64</code>	64-bit signed integer arrays
<code>uint8</code>	8-bit unsigned integer arrays
<code>uint16</code>	16-bit unsigned integer arrays
<code>uint32</code>	32-bit unsigned integer arrays
<code>uint64</code>	64-bit unsigned integer arrays

## The image transform

The orientation of the image with respect to the scanner axes is determined by the combination of the *image axes* and the *location of the corner voxel*. This information is encapsulated in the *transformation matrix*, commonly referred to simply as the *transform*. You can view the transform for any image using `cminfo`, for example:

```
>> cminfo('dwi.cmf')
*****
Locations:      /User/wuye/Testing/dwi.cmf
Dimensions:     104 x 104 x 54 x 167
Voxel size:     2.30769 x 2.30769 x 2.3 x 1
Data strides:   [ -1 -2 3 4 ]
Type:           Image
Data type:      Single
Intensity scaling: offset = 0, multiplier = 1
Transform:      0.9999      6.887e-09      -0.01564      -116.1
                -0.001242    0.9968        -0.07943      -89.44
                0.01559      0.07944        0.9967        -64.27
*****
```

The ‘Transform’ field above shows the first 3 rows of the transformation matrix (technically, this is a 4×4 matrix, but the last row is always set to [ 0 0 0 1 ]). The first 3 columns correspond to the *x*, *y* & *z* image axes respectively, while the last column corresponds to the location *in real (scanner/world) space* of the corner voxel (i.e. the voxel at index [ 0 0 0 ]).

In *COMEDI*, the transform shown always corresponds to the transformation from image coordinates *in millimeters* to scanner coordinates *in millimeters* - the voxel size is not taken into account, and the image axes are always normalised to unit amplitude. This may differ from other packages.

Furthermore, *COMEDI* will always present the transform that best matches the real space. If the transform of the image on file represents a large rotation, such that for example the first image axis is closer to the scanner’s *z* axis, this transform will be modified by permutation or inversion of the axes to bring it in alignment with the expected coordinate system, so that the first axis genuinely can be interpreted as approximately left-right, etc. To achieve this, *COMEDI* will also modify the image strides to match.

## 3.2.2 Supported image formats

This lists the various image formats currently supported by *COMEDI*.

**MRtrix image formats (.mih / .mif)**

**Compressed COMEDI image format (.cmf.gz)**

**DICOM (folder or .dcm)**

**NIfTI & NIfTI-2 (.nii)**

**Compressed NIfTI (.nii.gz)**

**FreeSurfer formats (.mgh / .mgz)**

**Analyse format (.img / .hdr)**

MRtrix Tracks file format (.tck)

MRtrix Track Scalar File format (.tsf)

Nearly Raw Raster Data (.nrrd/.nhdr)

## 3.3 List of COMEDI commands

### 3.3.1 dmridenoise

#### Synopsis

dMRI noise level estimation and denoising using Marchenko-Pastur PCA

#### Usage

```
>> dmridenoise(input,output,name=value)
```

- *input*: the input diffusion-weighted image.
- *output*: the output denoised DWI image.

#### Description

DWI data denoising and noise map estimation by exploiting data redundancy in the PCA domain using the prior knowledge that the eigenspectrum of random covariance matrices is described by the universal Marchenko-Pastur (MP) distribution. Fitting the MP distribution to the spectrum of patch-wise signal matrices hence provides an estimator of the noise level ‘sigma’, as was first shown in Veraart et al. (2016) and later improved in Cordero-Grande et al. (2019). This noise level estimate then determines the optimal cut-off for PCA denoising.

Important note: image denoising must be performed as the first step of the image processing pipeline. The routine will fail if interpolation or smoothing has been applied to the data prior to denoising.

Note that this function does not correct for non-Gaussian noise biases present in magnitude-reconstructed MRI images. If available, including the MRI phase data can reduce such non-Gaussian biases, and the command now supports complex input data.

#### Options

- **mask=image** Only process voxels within the specified binary brain mask image.
- **noise=image** The output noise map.
- **algorithm=** (Default=mppca) Below is a list of available denoise algorithms: *ghost*, *mppca*

## Standard options

- **force** (Default=false) force overwrite of output files (caution: using the same file as input and output might cause unexpected behaviour).
- **core=integer** (Default=0) use this number of threads in multi-threaded applications (set to 0 to disable multi-threading).

## References

Veraart, J.; Novikov, D.S.; Christiaens, D.; Ades-aron, B.; Sijbers, J. & Fieremans, E. Denoising of diffusion MRI using random matrix theory. *NeuroImage*, 2016, 142, 394-406, doi: 10.1016/j.neuroimage.2016.08.016

Veraart, J.; Fieremans, E. & Novikov, D.S. Diffusion MRI noise mapping using random matrix theory. *Magn. Res. Med.*, 2016, 76(5), 1582-1593, doi: 10.1002/mrm.26059

Cordero-Grande, L.; Christiaens, D.; Hutter, J.; Price, A.N.; Hajnal, J.V. Complex diffusion-weighted image estimation via matrix recovery under general noise models. *NeuroImage*, 2019, 200, 391-404, doi: 10.1016/j.neuroimage.2019.06.039

---

**Author:** Ye Wu ([amri.wuye@gmail.com](mailto:amri.wuye@gmail.com)) and Pew-Thian Yap ([ptyap@med.unc.edu](mailto:ptyap@med.unc.edu))

**Copyright:** Copyright (c) 2018-2021 the COMEDI contributors.

This Source Code Form is subject to the terms of the Mozilla Public License, v. 2.0. If a copy of the MPL was not distributed with this file, You can obtain one at <http://mozilla.org/MPL/2.0/>.

Covered Software is provided under this License on an “as is” basis, without warranty of any kind, either expressed, implied, or statutory, including, without limitation, warranties that the Covered Software is free of defects, merchantable, fit for a particular purpose or non-infringing. See the Mozilla Public License v. 2.0 for more details.

For more details, see <http://www.comedi.io/>.

## 3.3.2 dmrimask

### Synopsis

Generates a whole brain mask from a DWI image

### Usage

```
>> dmrimask(input,output,name=value)
```

- *input*: the input DWI image containing volumes that are both diffusion weighted and b=0
- *output*: the output whole-brain mask image



## Description

All diffusion weighted and b=0 volumes are used to obtain a mask that includes both brain tissue and CSF.

In a second step peninsula-like extensions, where the peninsula itself is wider than the bridge connecting it to the mask, are removed. This may help removing artefacts and non-brain parts, e.g. eyes, from the mask.

## Options

- **maxiter=integer** (Default=2) number of iterative
- **clean=integer** (Default=2) the maximum scale used to cut bridges. A certain maximum scale cuts bridges up to a width (in voxels) of 2x the provided scale. Setting this to 0 disables the mask cleaning step. (Default: 2)

## Standard options

- **force** (Default=false) force overwrite of output files (caution: using the same file as input and output might cause unexpected behaviour).
- **core=integer** (Default=0) use this number of threads in multi-threaded applications (set to 0 to disable multi-threading).

## References

Wu, Y., Y. Hong, W. Lin, P.-T. Yap. *Automated Identification of Non-Brain Voxels for Clean Brain Extraction Using Diffusion MRI*, ISMRM, Sydney, Australia, April 18-23, 2020.

Wu, Y., Ahmad, S., Huynh, K.M., Liu, S., Thung, KH., Lin, W., P.-T. Yap, 2021. *An Automated Processing Pipeline for Diffusion MRI in the Baby Connectome Project*, ISMRM, May 15-20, 2021.

**Author:** Ye Wu ([amri.wuye@gmail.com](mailto:amri.wuye@gmail.com)) and Pew-Thian Yap ([ptyap@med.unc.edu](mailto:ptyap@med.unc.edu))

**Copyright:** Copyright (c) 2018-2021 the COMEDI contributors.

This Source Code Form is subject to the terms of the Mozilla Public License, v. 2.0. If a copy of the MPL was not distributed with this file, You can obtain one at <http://mozilla.org/MPL/2.0/>.

Covered Software is provided under this License on an “as is” basis, without warranty of any kind, either expressed, implied, or statutory, including, without limitation, warranties that the Covered Software is free of defects, merchantable, fit for a particular purpose or non-infringing. See the Mozilla Public License v. 2.0 for more details.

For more details, see <http://www.comedi.io/>.









Lang	Command	Dependence	Synopsis
	cmdDwiFiberClustering		White matter tractography clustering
	cmdDwiFiberDecode		White fiber streamline decoding using the cosine basis functions
	cmdDwiFiberFilter		Perform various editing operations on White fiber streamline
	cmdDwiFiberEncode		White fiber streamline encoding using the cosine basis functions

Table 1 – continued from previous page

Lang	Command	Dependence	Synopsis
	cmdDwiFiberSmooth		White fiber streamline smoothing
	cmdDwiFiberStatis		Calculate statistics on streamlines
	cmdDwiGibbsRemoval		Remove Gibbs Ringing Artifacts from a DWI dataset
	cmdDwiNoiseRemoval		dMRI noise level estimation and denoising
	cmdDwiShellExtract		Extract diffusion-weighted volumes or certain shells from a DWI dataset
	cmdDwiShellMath		Apply an operation to each b-value shell in a DWI series
	cmdDwiSkullStripping		Generates a whole brain mask from a DWI image
	cmdFileConvert		Perform conversion between different file types
	cmdImageCompare		Computes a dissimilarity metric between two images
	cmdImageMath		Apply generic voxel-wise mathematical operations to images
	cmdImageRegister		Register two images together using a symmetric rigid, affine or non-linear
	cmdImageConcatenate		Concatenate several images into one
	cmdAnatGibbsRemoval		Remove Gibbs Ringing Artifacts from image
	cmdAnatHistogramMatch		Modify the intensities of one image to match the histogram of another
	cmdAnatHistogramMath		Generate a histogram of image intensities
	cmdImageCrop		Modify the grid of an image by cropping
	cmdImageFilter		Perform filtering operations on 3D / 4D MR images
	cmdImagePadding		Modify the grid of an image by padding
	cmdImageRegrid		Modify the grid of an image by regriding
	cmdAnatLabelConvert		Convert a connectome node image from one lookup table to another
	cmdAnatLabelFilter		Perform filtering operations on 3D / 4D mask images
	cmdAnatTissueSegment		Generate a set of tissue map
	cmdBidsLoad		Conversion of computational medical file

Table 1 – continued from previous page





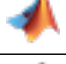

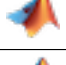

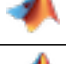

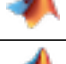




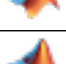



















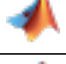



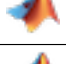

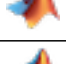






Lang	Command	Dependence	Synopsis
	cmdDwiBiasCorrect		Perform B1 field inhomogeneity correction for a DWI volume series
	cmdDwiConnectomeEstimate		Generate a connectome matrix from a streamlines file and a parcellation
	cmdDwiConnectomeNormalize		Normalization or filtering of connectome matrix
	cmdDwiConnectomeExtract		Extract streamlines from a tractogram based on their assignment to parcellation
	cmdDwiDirectionSampling		Generate a set of uniformly distributed directions on single-/multi-shell
	cmdDwiDirectionSplit		Split a set of evenly distributed directions into approximately uniformly distributed
	cmdDwiEddyCorrect	 	Perform diffusion image pre-processing using FSL's eddy tool; including
	cmdDwiFiberMapping		Use track data as a form of contrast for producing a high-resolution image
	cmdDwiFiberMeasure		Sample values of an associated image along tracks
	cmdDwiFiberRegister		Direct bundle registration
	cmdDwiFiberResample		Resample each streamline in a track file to a new set of vertices
	cmdDwiFiberSplit		Perform various editing operations on track files
	cmdDwiFiberTracking		Perform streamlines tractography
	cmdDwiFiberWarp		Apply a spatial transformation to a tracks file
	cmdDwiFodEstimate		Estimate fibre orientation distributions from diffusion data
	cmdDwiFodNormalize		Multi-tissue informed log-domain intensity normalisation
	cmdDwiFodPeaks		Extract the peaks of a spherical harmonic function in each voxel
	cmdDwiFodResponse		Estimate response function for spherical deconvolution
	cmdDwiFodRegister		Register the FOD image
	cmdDwiGradientCorrect		Check the orientation of the diffusion gradient table
	cmdDwiTensorEstimate		Diffusion tensor estimation
	cmdDwiKurtosisEstimate		Diffusion kurtosis estimation
	cmdDwiTissueSegment		Tissue segmentation using sparse non-negative matrix factorization of sp

Table 1 – continued from previous page

Lang	Command	Dependence	Synopsis
	cmdInfo		Display file header information
	cmdViewer		COMEDI viewer
	cmdClean		Clean up residual temporary files
	cmdInstall		Installation of COMEDI
	cmdSetup		Set up COMEDI
	cmdUpdate		Update COMEDI
	cmdDwiFiberFilterWithCommit		Filter a whole-brain fibre-tracking data set using COMMIT
	cmdDwiFiberTrackingWithDipy	 <b>DIPY</b>	Perform streamlines tractography using DIPY
	cmdInstallDipy	 <b>DIPY</b>	Installation of DIPY
	cmdInstallAmico		Installation of AMICO
	cmdInstallFsl	 	Installation of FSL
	cmdInstallMrtrix	 	Installation of MRtrix
	cmdInstallFreesurfer	 	Installation of Freesurfer
	cmdInstallAnts		Installation of ANTs
	cmdInstallCommit		Installation of COMMIT

## 3.4 An Automated Processing Pipeline for Diffusion MRI in the Baby Connectome Project

### 3.4.1 Abstract

Processing baby diffusion MRI (dMRI) data is challenging due to the low and spatially-varying diffusion anisotropy, rendering standard analysis techniques developed for adult data inapplicable. Here, we present a fully-automated processing pipeline for baby dMRI, tailored particularly to the data collected in the Baby Connectome Project (BCP).

The human brain is arguably the most complex system in biology and yet its macroscopic layout is nearly complete by the time of term birth. The infant brain develops rapidly during the first years of life, posing significant challenges to precise quantification of rapid dynamic changes that occur during this critical period of brain development.

The increasing availability of longitudinal baby MRI data, such as those acquired through the Baby Connectome Project (BCP), affords unprecedented opportunity for precise charting of early brain developmental trajectories in order to understand normative and aberrant growth.

We describe here an automated processing pipeline for baby dMRI, consisting of (i) image quality control (IQC) for distinguishing between good and poor quality data, (ii) anatomy-guided correction for eddy-current and susceptibility-induced distortions, (iii) tissue microstructural analysis, and (iv) reconstruction of white matter (WM) pathways.

### 3.4.2 Methods

#### DMRI acquisition

In the BCP, diffusion-weighted (DW) images were acquired using Siemens 3T Magnetom Prisma MRI scanners with a  $140 \times 140 \times 140$  mm<sup>3</sup> imaging matrix,  $1.5 \times 1.5 \times 1.5$  mm<sup>3</sup> resolution,  $TE=88$  ms,  $TR=2,365$  ms, 32-channel receiver coil, and  $b=500, 1000, 1500, 2000, 2500, 3000$  s/mm<sup>2</sup>, covered by a total of 144 noncollinear gradient directions for either posterior-anterior or anterior-posterior phase-encoding directions (PEDs). 6 non-DW images were collected for each PED.

#### Image quality control (IQC)

The DW images are annotated as “pass” (no/minor artifacts), “questionable” (moderate artifacts), or “fail” (heavy artifacts). The IQC framework utilizes a nonlocal residual network to first examine the quality of each imaging slice. Slice-level features are then agglomerated for volume-level quality assessment, which is in turn used to arrive at the assessment outcome at the subject-level. Subjects annotated as “fail” are excluded from subsequent processing and analysis.

#### Distortion correction

The DW images associated with each PED are first corrected for eddy-current distortion by affine registration followed by coarse deformable registration to their corresponding non-DW image using ANTs. To correct for susceptibility-induced distortion, we first compute the spherical mean images (SMIs) of the eddy-current corrected DW images, and jointly register the SMIs of all shells and the non-DW images to the corresponding aligned T1-weighted (T1w) and T2-weighted (T2w) images. The corrected DW images for both PEDs are obtained by one-time warping of the original DW images via composed deformation fields. Finally, the warped DW images for opposite PEDs are combined via the signal harmonic mean.

#### Tissue microstructure

A recent method called spherical mean spectrum imaging (SMSI) is used to quantify tissue microarchitecture. SMSI allows a wide variety of features, such as intracellular volume fraction (ICVF), extracellular volume fraction (ECVF), free-water volume fraction, intra-soma volume fraction, anisotropy, and orientation coherence index, to be computed for comprehensive microstructural analysis. SMSI characterizes the whole fine- to coarse-scale diffusion spectrum and is hence well suited for capturing dynamic microstructural changes in the baby brain. SMSI has been recently demonstrated to show greater sensitivity to developmental changes via a multivariate framework, revealing distinct longitudinal patterns of both cortical and subcortical areas.

## White matter pathways

WM tractography is generated by fiber tracking using super-resolution asymmetry spectrum imaging (ASI). ASI fits a mixture of asymmetric fiber orientation distribution function (FODF) to the diffusion signal. WM tractograms are then generated by successively following local directions determined from the FODFs. ASI-based tractography mitigates the gyral bias problem common in existing tractography algorithms and improves cortico-cortical connectivity in the baby brain. We employ TractDL for fast and robust identification of fiber bundles of interest from a large number of streamlines. More than 160 anatomical WM pathways are identified consistently.

### 3.4.3 References

1. Wu, Y., Ahmad, S., Huynh, K.M., Liu, S., Thung, K.H., Lin, W., P.-T. Yap, 2021. *An Automated Processing Pipeline for Diffusion MRI in the Baby Connectome Project*, ISMRM, May 15-20, 2021.

## 3.5 Subsampling Diffusion Gradients via Poisson Sphere Elimination

### 3.5.1 Abstract

Subsampling from a set of diffusion gradient directions is useful for evaluation of image acquisition and reconstruction strategies. However, a challenge associated with gradient subsampling is the requirement to ensure uniform distribution of a predetermined number of subsampled directions. Here, we introduce a method for near-uniform subsampling for an arbitrary target number of gradient directions.

Gradient subsampling requires the outcome to be ideally uniformly distributed for a target number of directions. Few methods have been proposed to tackle this problem. One approach is to select the gradient directions for each shell based on a smaller set of reference directions that are uniformly distributed. Another approach is to split a set of directions into subsets that are approximately uniformly distributed via iterative permutations. However, it is not straightforward using this method to choose a target number of output directions. In this work, we introduce a method for fast subsampling with an arbitrary target number of gradient directions without the need for reference directions or iterative optimization.

### 3.5.2 Methods

We employ Poisson sphere sample elimination for gradient subsampling.

**Single-Shell Subsampling:** With a desired Poisson sphere radius, a dart-throwing mechanism is used to determine whether each sample, in the order of increasing index, should be accepted or eliminated based on its distance to previously accepted samples. When two samples are close together, dart-throwing eliminates the sample with the greater index. Hence, given a set of samples in a particular order, dart-throwing picks a subset with an arbitrary size. To avoid explicitly specifying the Poisson sphere radius, we employ a greedy sample elimination algorithm to compute a weight for each sample in a given set and then eliminate the samples with weights greater than a threshold.

**Multi-Shell Subsampling:** We extend the above method to multi-shell subsampling with an arbitrary target number of gradient directions for each shell. For each sample in a shell, we can compute an intra-shell distance between the sample and the other samples in the same shell, and an inter-shell distance between the sample and the other samples in all shells collapsed into a single shell. We use a weighted combination of the two distances to select samples via Poisson sphere sample elimination. The optimal weight for distance combination is determined based on the minimum error between the spherical mean images computed with the subsampled directions and the original directions.

### 3.5.3 References

1. Wu, Y., Ahmad, S., Ma, L., Yang, E., P.-T. Yap, 2021. *Subsampling Diffusion Gradients via Poisson Sphere Elimination*, ISMRM, May 15-20, 2021.
2. Yuksel C. Sample Elimination for Generating Poisson Disk Sample Sets. *Comput Graph Forum*. 2015;34: 25–32.
3. Bridson R. Fast Poisson disk sampling in arbitrary dimensions. *SIGGRAPH sketches*. 2007;10: 1.

## 3.6 Super-Resolution Asymmetry Spectrum Imaging (SR-ASI)

### 3.6.1 Abstract

We introduce a technique for super-resolution reconstruction of diffusion MRI, harnessing fiber-continuity (FC) as a constraint in a global whole-brain optimization framework. FC is a biologically-motivated constraint that relates orientation information between neighboring voxels. We show that it can be used to effectively constrain the inverse problem of recovering high-resolution data from low-resolution data. Since voxels are inter-related by FC, we devise a global optimization framework that allows solutions pertaining to all voxels to be solved simultaneously.

### 3.6.2 Methods

The low resolution (LR) DW volumes are considered as down-sampled versions of high resolution (HR) DW volumes that need to be estimated. For this purpose, we let  $\mathbf{Y} \in \mathbb{R}^{N_v \times M_g}$  denote a set of LR DW volumes with  $N_v$  voxels per volume and  $M_g$  gradient directions across different shells. The LR volumes  $\mathbf{Y}$  are related to the HR volumes  $\mathbf{S} \in \mathbb{R}^{M_v \times M_g}$  by  $\mathbf{Y} = \mathbf{D}\mathbf{S} + \boldsymbol{\mu}$ , where  $\mathbf{D}$  is a down-sampling matrix that averages neighboring voxels and  $\boldsymbol{\mu}$  denotes noise. The sampling of  $\mathbf{Y}$  can be encoded by a binary matrix  $\mathbf{B}$  such that  $\mathbf{B} \odot \mathbf{Y} = \mathbf{B} \odot (\mathbf{D}\mathbf{S} + \boldsymbol{\mu})$ , where  $\odot$  is the element-wise multiplication operator. The model is general and can account for different spatio-angular subsampling schemes determined by  $\mathbf{B}$  and  $\mathbf{D}$ .

Our method uses fiber continuity across voxels to regularize the inverse problem of recovering the HR volumes. Fiber continuity is a natural constraint supporting the fact that orientations should be consistent along fiber tracts. A model based on asymmetric fiber orientation distribution functions (AFODFs) is used to represent the sub-voxel configurations. In DMRI, the signal profile is typically assumed to be antipodal symmetric, implying that orientation in a positive hemisphere is always identical to its counterpart in the negative hemisphere. Symmetric FODFs are not sufficient in regions with fanning and bending fiber trajectories. To improve sub-voxel fiber continuity, we estimate AFODFs by incorporating information from neighboring voxels, allowing FODF asymmetry to better represent complex configurations {Cetin\_Karayumak2018-om, Bastiani2017-hm, Reisert2012-xo}. The discontinuity of AFODFs,  $\mathcal{F}_{\text{aniso}}$ , over all voxels and directions ( $\mathbf{u} \in \mathbb{S}^2$ ) is measured as  $\Phi(\mathcal{F}_{\text{aniso}}) = \int_{\mathbf{u} \in \mathbb{S}^2} \|\mathcal{F}_{\text{aniso}}(\mathbf{u}) \otimes \mathbf{W}(\mathbf{u}) - \mathcal{F}_{\text{aniso}}(\mathbf{u})\|_{\text{F}}^2 d\mathbf{u}$ , where  $\mathbf{W}$  is a normalized directional probability distribution function as defined in {Wu2020-ox} and  $\otimes$  is a column-wise multiplication operator.

We use a multi-tissue spherical convolution model to represent the diffusion signal at each voxel of  $\mathbf{S}$ . Specifically,  $\mathbf{S}$  can be decomposed as  $\mathbf{S} = \mathcal{R}\mathcal{X}$ , with  $\mathcal{R} = [\mathbf{R}_{\text{aniso}}, \mathbf{R}_{\text{aniso}}, \mathbf{R}_{\text{iso},1}, \dots, \mathbf{R}_{\text{iso},n}]$  being the multi-tissue axially symmetric response function (RF) consisting of an anisotropic component  $\mathbf{R}_{\text{aniso}}$  and  $n$  isotropic compartments  $\{\mathbf{R}_{\text{iso},i}\}_{i=1}^n$  as defined in {Wu2019-pe}. Each column of  $\mathcal{X} = [\mathbf{X}_{\text{aniso}}^+, \mathbf{X}_{\text{aniso}}^-, \mathbf{X}_{\text{iso},1}, \dots, \mathbf{X}_{\text{iso},n}]^T$  represents the spherical harmonics (SH) coefficients of AFODF at each voxel location. The AFODF is represented by two sets of even-order spherical harmonics {Wu2020-ox}, capturing potentially asymmetric sub-voxel fiber configurations. That

is,  $\mathcal{F}_{\text{aniso}}(\mathbf{u}) = \begin{cases} \mathbf{A}(\mathbf{u}) \cdot \mathbf{X}_{\text{aniso}}^+, & \mathbf{u} \in \mathbb{S}_+^2, \\ \mathbf{A}(\mathbf{u}) \cdot \mathbf{X}_{\text{aniso}}^-, & \mathbf{u} \in \mathbb{S}_-^2, \end{cases}$  where  $\mathbf{A}(\mathbf{u})$  is the real even-order SH basis function sampled in direction

$\mathbf{u}$ , and the column vectors of  $\mathbf{X}_{\text{aniso}}^+$  and  $\mathbf{X}_{\text{aniso}}^-$  are the corresponding SH coefficients for the positive and negative hemispheres ( $\mathbb{S}_+^2$  and  $\mathbb{S}_-^2$ ).



Based on Eq. [eq:sr](#), we estimate  $\mathbf{S}$  and  $\mathcal{X}$  by solving  $\min_{\mathbf{S}, \mathcal{X}} \frac{1}{2} \|\mathbf{B} \odot (\mathbf{Y} - \mathbf{DS})\|^2 + \lambda \|\mathcal{L}\mathcal{X}\|^2$ ,

$$\text{s.t. } \begin{cases} \mathbf{S} = \mathcal{R}\mathcal{X}, \\ \mathcal{A}\mathcal{X} \succeq 0, \\ \Phi(\mathcal{F}_{\text{aniso}}) \leq \epsilon, \\ \mathbf{S} \succeq 0, \end{cases} \quad \text{where the Laplace-Beltrami regularization \{Tournier2007-kg\} is realized via } \mathcal{L} =$$

$\text{diag}[\mathbf{L}, \mathbf{L}, 0, \dots, 0]$  where  $\mathbf{L}_{jj} = \ell_j(\ell_j + 1)$  with  $\ell_j$  being the order associated with the  $j$ -th coefficient.  $\lambda$  is the regularization parameter and the matrix  $\mathcal{A} = \text{diag}[\mathbf{A}, \mathbf{A}, a_0, \dots, a_0]$  maps the SH coefficients  $\mathcal{X}$  to the AFODF amplitudes for imposing AFODF non-negativity.  $a_0 = \sqrt{\frac{1}{4\pi}}$  is the 0-th order SH basis function. Problem [eq:model2](#) is solved using alternating direction method of multipliers (ADMM). Specifically, the problem can be cast as a strictly convex quadratic programming (QP) problem, which can be solved by an operator splitting solver for quadratic programs (OSQP) [Stellato2020-fp](#). Following common super-resolution frameworks [Shi2015-dv, Ning2016-kk, Lum2015-wk](#), we used linearly interpolated data to initialize ADMM.

The WM RF is estimated for each b-shell from the average of the reoriented diffusion signal profiles of voxels with high anisotropy in WM. Also, isotropic RFs are set with diffusivity values ranging from  $0.1 \times 10^{-3} \text{ mm}^2/\text{s}$  to  $3 \times 10^{-3} \text{ mm}^2/\text{s}$  and step size  $0.2 \times 10^{-3} \text{ mm}^2/\text{s}$ . This will allow better characterization of tissue microstructure in infant brain.

We used k-fold cross-validation to determine the optimal regularization parameter  $\lambda$  in [eq:model2](#). Two thousand random WM voxels from an BCP DMRI dataset and 61 candidate values for  $\lambda$ , logarithmically spanning the interval between 0.01 and 10, were considered [Wu2020-vl, Wu2020-jq, Wu2020-vl, Bastiani2017-hm](#). We found that the optimal value was 0.01. This value was applied to all experiments. The method is publicly available as part of the Computational Medical Imaging Toolkit ([url\{https://www.comedi.io\}](https://www.comedi.io)).

### 3.6.3 References

1. Wu, Y., Lin, W., Shen, D., Yap, P.-T., Consortium, U.B.C.P., others, 2019d. *Asymmetry Spectrum Imaging for Baby Diffusion Tractography*, in: International Conference on Information Processing in Medical Imaging. Springer, pp. 319–331.
2. Wu, Y., Lin, W., Shen, D., Yap, P.-T., 2019b. *Improving Tractography in Baby Diffusion MRI via Asymmetric Spectrum Imaging*, in: Proceedings of the International Society of Magnetic Resonance in Medicine (ISMRM).
3. Wu, Y., Hong, Y., Ahmad, S., Chang, W., Lin, W., Shen, D., Yap, P.-T. 2020. *Globally Optimized Super-Resolution of Diffusion MRI Data via Fiber Continuity*, in: International Conference on Information Processing in Medical Imaging.

## 3.7 Active Cortex Tractography (ACT)

### 3.7.1 Abstract

Most existing diffusion tractography algorithms are affected by gyral bias, causing the termination of streamlines at gyral crowns instead of sulcal banks. We propose a tractography technique, called active cortex tractography (ACT), to overcome gyral bias by enabling fiber streamlines to curve naturally into the cortex. We show that the cortex can play an active role in cortical tractography by providing anatomical information to overcome orientation ambiguities as the streamlines enter the superficial white matter in gyral blades and approach the cortex. This is achieved by devising a direction scouting mechanism that takes into account the white matter surface normal vectors. The scouting mechanism allows probing of directions further in space to prepare the streamlines to turn at appropriate angles. The surface normal vectors guide the streamlines to turn into the cortex, perpendicular to the white-gray matter interface.



### 3.7.2 Methods

**Deterministic tractography methods** cite{Basser2000-ju,Tournier2012-hk,Mori1999-ct} typically reconstruct fiber streamlines by

$$\mathbf{r}_{i+1} = \mathbf{r}_i + \rho \mathbf{t}_i,$$

where  $\mathbf{r}_0$  is a given seed point, and the streamline  $\mathcal{X} = [\mathbf{r}_0, \dots, \mathbf{r}_n]$  is estimated using a fixed step size  $\rho$ . The forward direction  $\mathbf{t}_i$  is typically chosen from  $M$  directions  $\{\mathbf{d}_1, \dots, \mathbf{d}_M\}$  that correspond to the local maxima of the fiber orientation distribution function (FODF) cite{Jeurissen2019-qh} in the voxel containing  $\mathbf{r}_i$ , minimizing the angular deviation with respect to the previous direction  $\mathbf{t}_{i-1}$ :

$$\mathbf{t}_i = \underset{\mathbf{d}}{\operatorname{argmin}} \arccos(\mathbf{t}_{i-1} \cdot \mathbf{d}), \quad \mathbf{d} \in \{\mathbf{d}_1, \dots, \mathbf{d}_M\}, \quad \text{s.t. } \arccos(\mathbf{t}_{i-1} \cdot \mathbf{d}) \leq \theta,$$

where the maximum allowed angular deviation is  $\theta$ . FODFs are typically assumed to be antipodally symmetric; hence the configurations, such as fanning and bending, cannot be represented correctly.

We propose a tractography method to adaptively update the forward direction and the step size based on the asymmetric fiber orientation distribution (AFODF). We further incorporate surface prior to help the streamlines bend more naturally in gyral blades into the cortex.

Estimating sub-voxel fiber orientations in gyral blades is challenging due to the fanning and bending configurations. Asymmetric FODFs cite{wu2018multi,bastiani2017improved,Wu2020-ce} have been shown to improve tractography in gyral blades by explicitly considering sub-voxel orientation asymmetry and continuity across neighboring voxels. Let  $\mathbb{U}_{(\mathbf{r}, \mathbf{n})}$  be the voxel subspace defined by the position vector  $\mathbf{r}$  with the normal vector  $\mathbf{n}$ . Then, with an asymmetric FODF  $\mathcal{F}$ , the forward direction  $\mathbf{t}_i$  can be determined in voxel subspace  $\mathbb{U}$  (see Fig.~ref{fig:space}, Left):

$$\mathbf{t}_i = \underset{\mathbf{t}^* \in \mathbb{U}}{\operatorname{argmax}} \mathcal{F}_{\mathbf{r}_i}(\mathbf{t}^*), \quad \mathbb{U} := \mathbb{U}_{(\hat{\mathbf{r}}_i, \mathbf{r}_i - \hat{\mathbf{r}}_i)} \cap \mathbb{U}_{(\hat{\mathbf{r}}_i, \mathbf{t}_{i-1})},$$

where  $\mathbb{U}_{(\hat{\mathbf{r}}_i, \mathbf{r}_i - \hat{\mathbf{r}}_i)}$  is the voxel subspace containing  $\mathbf{r}_i$  and  $\mathbb{U}_{(\hat{\mathbf{r}}_i, \mathbf{t}_{i-1})}$  is the voxel subspace defined by the previous direction  $\mathbf{t}_{i-1}$  and the current position  $\hat{\mathbf{r}}_i$ .

**Unlike conventional tractography algorithms in which the forward direction depends only on the fiber peaks at the current position**

$$\tilde{\mathbf{t}}_i = \delta_i \mathbf{t}_i + \delta_{i+1} \mathbf{t}_{i+1},$$

**where  $\delta_i = \rho \mathcal{F}_{\mathbf{r}_i}(\mathbf{t}_i)$ . Then, the next position  $\mathbf{r}_{i+1}$  is updated with the adaptive step size:  $\mathbf{r}_{i+1} = \mathbf{r}_i + \delta_i \tilde{\mathbf{t}}_i$ .**

We harness the anatomical information provided by the cortex to guide the tracking of the streamline when it enters the gyral blade and into the cortex. This is achieved by updating the forward direction by

$$\tilde{\mathbf{t}}_i \leftarrow \tilde{\mathbf{t}}_i + \exp(-\|\mathbf{r}_i - \mathbf{p}_i\|) \mathbf{v}_i,$$

**where  $\mathbf{p}_i$  is a vertex on the WM surface with normal vector  $\mathbf{v}_i$ , which is chosen such that  $\{\mathbf{p}_i, \mathbf{v}_i\} = \underset{\mathbf{p}, \mathbf{v}}{\operatorname{argmin}} \exp(-\|\mathbf{r}_i - \mathbf{p}\|) \arccos(\mathbf{v} \cdot \tilde{\mathbf{t}}_i), \quad \mathbf{v} \in \mathbb{V},$**

and  $\mathbb{V}$  is a field of surface normals (see Fig.~ref{fig:surface}). The sign of the normal vector is flipped when the streamline leaves the cortex into superficial WM:

$$\mathbf{v}_i = \begin{cases} \mathbf{v}_i, & \text{if } \arccos(\mathbf{v}_i \cdot \tilde{\mathbf{t}}_i) \leq \frac{\pi}{2}, \\ -\mathbf{v}_i, & \text{if } \arccos(\mathbf{v}_i \cdot \tilde{\mathbf{t}}_i) > \frac{\pi}{2}. \end{cases}$$

### 3.7.3 References

1. Wu, Y., Hong, Y., Ahmad, S. and Yap, P.T., 2021, September. Active Cortex Tractography. In International Conference on Medical Image Computing and Computer-Assisted Intervention (pp. 467-476). Springer, Cham.

## 3.8 White Matter Tract Atlases of a Century of Human Life

### 3.8.1 Abstract

The brain's white matter (WM) evolves at a rapid pace during childhood and adolescence, stabilizes during young and middle adulthood, and degenerates in late adulthood. Here, we introduce a set of white matter tract atlases spanning birth to 100 years of age, covering 215 WM bundles to facilitate quantification of WM changes across the entire human lifespan. To our knowledge, this is to date the most comprehensive set of atlases, covering the largest time span with the largest number of WM bundles.

### 3.8.2 Methods

In order to build WM tract atlases, we used MRI data from the Lifespan Human Connectome Projects (HCPs): (i) Baby Connectome Project (BCP, 0-5 years; Howell B.R. 2019); (ii) HCP Development (HCP-D, 8-21 years; Somerville L.H. 2018); (iii) HCP Young Adult (HCP, 22-37 years; Essen D.C.V 2013); and (iv) HCP Aging (HCP-A, 36-100 years; Bookheimer S.Y. 2019).

WM tractography was performed using super-resolution asymmetry spectrum imaging (ASI; Wu Y. 2019, 2020a, 2020b). ASI fits a mixture of asymmetric fiber orientation distribution function (FODF) to the diffusion signal. WM tractograms were then generated by successively following local directions determined from the FODFs. ASI-based tractography mitigates the gyral bias problem (Wu Y. 2019, 2020a) common in existing tractography algorithms and improves cortico-cortical connectivity. The fiber streamlines of each subject were warped to the atlas space via affine and nonlinear transforms estimated between the tissue map of the subject and an age-specific atlas. We employed TractDL (Wu Y. 2020c) to identify a total of 215 fiber bundles from the streamlines. The bundles were annotated anatomically following previous studies (Yeh F-C. 2018; Zhang F. 2018), yielding (i) 42 association pathways; (ii) 18 cerebellar pathways; (iii) 13 commissural pathways; (iv) 14 cranial nerve pathways; (v) 14 brainstem pathways; (vi) 98 projection pathways; and (vii) 16 superficial pathways.

We investigated the change of the relative volume of each tract bundle across the entire life span. For each bundle, the volume was computed by (i) counting the number of streamlines traversing each voxel, (ii) normalizing the streamline count for each with respect to the total number of streamlines in the bundle, and (ii) computing the volume sum of the voxels traversed by the tract bundle, with each voxel weighted by the normalized streamline count.

### 3.8.3 References

1. Wu, Y., Ahmad, S., Lin, W., Yap, P.-T., 2021. *White Matter Tract Atlases of a Century of Human Life*, in: OHBM, Virtual Meeting, 21-25 June, 2021.

---

## 3.9 Publications

## 3.10 Contributors

## 3.11 License and warranty

---

**Tip:** Copyright (c) 2021 Ye Wu All rights reserved.

Permission is hereby granted, free of charge, to any person obtaining a copy of this software and associated documentation files (the “Software”), to deal in the Software without restriction, including without limitation the rights to use, copy, modify, merge, publish, distribute, sublicense, and/or sell copies of the Software, and to permit persons to whom the Software is furnished to do so, subject to the following conditions:

The above copyright notice and this permission notice shall be included in all copies or substantial portions of the Software.

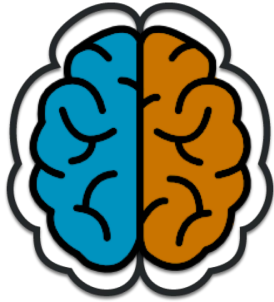
THE SOFTWARE IS PROVIDED “AS IS”, WITHOUT WARRANTY OF ANY KIND, EXPRESS OR IMPLIED, INCLUDING BUT NOT LIMITED TO THE WARRANTIES OF MERCHANTABILITY, FITNESS FOR A PARTICULAR PURPOSE AND NONINFRINGEMENT. IN NO EVENT SHALL THE AUTHORS OR COPYRIGHT HOLDERS BE LIABLE FOR ANY CLAIM, DAMAGES OR OTHER LIABILITY, WHETHER IN AN ACTION OF CONTRACT, TORT OR OTHERWISE, ARISING FROM, OUT OF OR IN CONNECTION WITH THE SOFTWARE OR THE USE OR OTHER DEALINGS IN THE SOFTWARE.

---

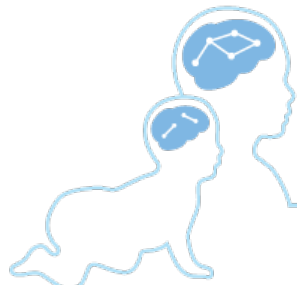
**Warning:** This tutorial is not intended to show the optimal or even recommended way of processing. It is merely a simplified example, intended to familiarise the user with the typical command line interface of certain basic processing steps.

This tutorial will hopefully provide enough information for a novice user to get from the raw DW image data to performing some streamlines tractography. It may also be useful for experienced COMEDI users in terms of identifying some of the new command names.

## 3.12 Acknowledgements



National Institutes  
of Health



BABY a UNC / UMN collaboration  
Connectome Project

---



BRIC

---

BIOMEDICAL RESEARCH  
IMAGING CENTER



## 3.13 Contact us

- Please contact [amri.wuye@gmail.com](mailto:amri.wuye@gmail.com) for questions and feedback.

---

**Note:** Please join us with [discussions](#) and [gitter](#)

---



## BIBLIOGRAPHY

- [Windows] [https://www.comedi.io/matlab/64/MCR\\_R2021b\\_win64\\_installer.zip](https://www.comedi.io/matlab/64/MCR_R2021b_win64_installer.zip)
- [Linux] [https://www.comedi.io/matlab/64/MCR\\_R2021b\\_glnxa64\\_installer.zip](https://www.comedi.io/matlab/64/MCR_R2021b_glnxa64_installer.zip)
- [MacOS] [https://www.comedi.io/matlab/64/MCR\\_R2021b\\_maci64\\_installer.zip](https://www.comedi.io/matlab/64/MCR_R2021b_maci64_installer.zip)
- [Binaries] <https://www.comedi.io/download>
- [Release] <https://github.com/diffusionmri/COMEDI/releases>
- [Release] <https://github.com/diffusionmri/comedi>
- [Ahmad2020] Ahmad, Sahar, Ye Wu, Khoi Minh Huynh, Kim-Han Thung, Weili Lin, Dinggang Shen, and Pew-Thian Yap. 2020. *Fast Correction of Eddy-Current and Susceptibility-Induced Distortions Using Rotation-Invariant Contrasts*. In Medical Image Computing and Computer Assisted Intervention – MICCAI 2020, 34–43. Springer, Cham.
- [Hong2020] Hong, Yoonmi, Wei-Tang Chang, Geng Chen, Ye Wu, Weili Lin, Dinggang Shen, and Pew-Thian Yap. 2020. *Multifold Acceleration of Diffusion MRI via Slice-Interleaved Diffusion Encoding (SIDE)*. arXiv [physics.med-ph]. arXiv. <http://arxiv.org/abs/2002.10908>.
- [Huynh2019a] Huynh, Khoi Minh, Geng Chen, Ye Wu, Dinggang Shen, and Pew-Thian Yap. 2019. *Multi-Site Harmonization of Diffusion MRI Data via Method of Moments*. IEEE Transactions on Medical Imaging 38 (7): 1599–1609.
- [Huynh2019b] Huynh, Khoi Minh, Jaeil Kim, Geng Chen, Ye Wu, Dinggang Shen, and Pew-Thian Yap. 2019. *Longitudinal Harmonization for Improving Tractography in Baby Diffusion MRI*. In Computational Diffusion MRI, 183–91. Springer, Cham.
- [Huynh2020a] Huynh, Khoi Minh, Ye Wu, Kim-Han Thung, Sahar Ahmad, Hoyt Patrick Taylor IV, Dinggang Shen, and Pew-Thian Yap. 2020. *Characterizing Intra-Soma Diffusion with Spherical Mean Spectrum Imaging*. In Medical Image Computing and Computer Assisted Intervention – MICCAI 2020, 354–63. Springer, Cham.
- [Huynh2019d] Huynh, Khoi Minh, Ye Wu, Kim-Han Thung, Geng Chen, Weili Lin, Dinggang Shen, and Pew-Thian Yap. 2019. *Biases of Microstructure Models in Baby Diffusion MRI*. In Proceedings of the International Society of Magnetic Resonance in Medicine (ISMRM).
- [Huynh2019e] Huynh, Khoi Minh, Tiantian Xu, Ye Wu, Geng Chen, Kim-Han Thung, Haiyong Wu, Weili Lin, Dinggang Shen, and Pew-Thian Yap. 2019. *Probing Brain Micro-Architecture by Orientation Distribution Invariant Identification of Diffusion Compartments*. In Medical Image Computing and Computer Assisted Intervention – MICCAI 2019, 547–55. Springer, Cham.
- [Huynh2020b] Huynh, Khoi Minh, Tiantian Xu, Ye Wu, Kim-Han Thung, Geng Chen, Weili Lin, Dinggang Shen, and Pew-Thian Yap. 2019. *Characterizing Non-Gaussian Diffusion in Heterogeneously Oriented Tissue*

- Microenvironments*. In Medical Image Computing and Computer Assisted Intervention – MICCAI 2019, 556–63. Springer, Cham.
- [Huynh2020c] Huynh, Khoi Minh, Tiantian Xu, Ye Wu, Xifeng Wang, Geng Chen, Haiyong Wu, Kim-Han Thung, Weili Lin, Dinggang Shen, and Pew-Thian Yap. 2020. *Probing Tissue Microarchitecture of the Baby Brain via Spherical Mean Spectrum Imaging*. IEEE Transactions on Medical Imaging 39 (11): 3607–18.
- [Li2019] Li, Guoshi, Yujie Liu, Yanting Zheng, Ye Wu, Pew-Thian Yap, Shijun Qiu, Han Zhang, and Dinggang Shen. 2019. *Identification of Abnormal Circuit Dynamics in Major Depressive Disorder via Multiscale Neural Modeling of Resting-State fMRI*. In International Conference on Medical Image Computing and Computer-Assisted Intervention, 682–90. Springer, Cham.
- [Liu2019] Liu, Feihong, Jun Feng, Geng Chen, Ye Wu, Yoonmi Hong, Pew-Thian Yap, and Dinggang Shen. 2019. *DeepBundle: Fiber Bundle Parcellation with Graph Convolution Neural Networks*. In Graph Learning in Medical Imaging, 88–95. Springer, Cham.
- [MaierHein2017] Maier-Hein, Klaus H., Peter F. Neher, Jean-Christophe Houde, Marc-Alexandre Cote, Eleftherios Garyfallidis, Jidan Zhong, Maxime Chamberland, et al. 2019. *The Challenge of Mapping the Human Connectome Based on Diffusion Tractography (vol 8, 1349, 2017)*. Nature Communications 10.
- [Nath2017] Nath, Vishwesh, Kurt G. Schilling, Prasanna Parvathaneni, Yuankai Huo, Justin A. Blaber, Allison E. Hainline, Muhamed Barakovic, et al. 2020. *Tractography Reproducibility Challenge with Empirical Data (TrACED): The 2017 ISMRM Diffusion Study Group Challenge*. Journal of Magnetic Resonance Imaging: JMIR 51 (1): 234–49.
- [Sun2019] Sun, Peng, Ye Wu, Geng Chen, Jun Wu, Dinggang Shen, and Pew-Thian Yap. 2019. *Tissue Segmentation Using Sparse Non-Negative Matrix Factorization of Spherical Mean Diffusion MRI Data*. In Computational Diffusion MRI, 69–76. Springer, Cham.
- [Taylor2019] Taylor, Hoyt Patrick, IV, Zhengwang Wu, Ye Wu, Dinggang Shen, Han Zhang, and Pew-Thian Yap. 2019. *Automated Parcellation of the Cortex Using Structural Connectome Harmonics*. In Medical Image Computing and Computer Assisted Intervention – MICCAI 2019, 475–83. Springer.
- [Wu2015a] Wu, Ye, Yuanjing Feng, Fei Li, and Carl Fredrik Westin. 2015. *Global Consistency Spatial Model for Fiber Orientation Distribution Estimation*. In 2015 IEEE 12th International Symposium on Biomedical Imaging (ISBI), 1180–83. IEEE.
- [Wu2018a] Wu, Ye, Yuanjing Feng, Dinggang Shen, and Pew-Thian Yap. 2018a. *A Multi-Tissue Global Estimation Framework for Asymmetric Fiber Orientation Distributions*. In Medical Image Computing and Computer Assisted Intervention – MICCAI 2018, 45–52. Springer, Cham.
- [Wu2020a] Wu, Ye, Yoonmi Hong, Sahar Ahmad, Wei-Tang Chang, Weili Lin, Dinggang Shen, and Pew-Thian Yap. 2020. *Globally Optimized Super-Resolution of Diffusion MRI Data via Fiber Continuity*. In Medical Image Computing and Computer Assisted Intervention – MICCAI 2020, 260–69. Springer, Cham.
- [Wu2020b] Wu, Ye, Yoonmi Hong, Sahar Ahmad, Weili Lin, Dinggang Shen, and Pew-Thian Yap. 2020. *Tract Dictionary Learning for Fast and Robust Recognition of Fiber Bundles*. In Medical Image Computing and Computer Assisted Intervention – MICCAI 2020, 251–59. Springer, Cham.
- [Wu2020c] Wu, Ye, Yoonmi Hong, Sahar Ahmad, Weili Lin, and Pew-Thian Yap. n.d. *White Matter Tract Atlases of the Baby Brain*.
- [Wu2020d] Wu, Ye, Yoonmi Hong, Yuanjing Feng, Dinggang Shen, and Pew-Thian Yap. 2020. *Mitigating Gyral Bias in Cortical Tractography via Asymmetric Fiber Orientation Distributions*. Medical Image Analysis 59 (January): 101543.
- [Wu2019a] Wu, Ye, Weili Lin, Dinggang Shen, and Pew-Thian Yap. 2019a. *Improving Tractography in Baby Diffusion MRI via Asymmetric Spectrum Imaging*. In Proceedings of the International Society of Magnetic Resonance in Medicine (ISMRM).



- [Wu2019b] Wu, Ye, Weili Lin, Dinggang Shen, Pew-Thian Yap, Unc/umn Baby Connectome Project Consortium, and Others. 2019. *Asymmetry Spectrum Imaging for Baby Diffusion Tractography*. In International Conference on Information Processing in Medical Imaging, 319–31. Springer, Cham.
- [Wu2014] Wu, Ye, Youyou Xu, Yuanjing Feng, Chengfeng Gao, and Fei Li. 2014. *A New Model-Based Spherical Deconvolution Method for Multi-Fiber Reconstruction*. In 2014 9th IEEE Conference on Industrial Electronics and Applications, 1456–60. IEEE.
- [Wu2018b] Wu, Ye, Fan Zhang, Nikos Makris, Yuping Ning, Isaiah Norton, Shenglin She, Hongjun Peng, et al. 2018. *Investigation into Local White Matter Abnormality in Emotional Processing and Sensorimotor Areas Using an Automatically Annotated Fiber Clustering in Major Depressive Disorder*. *NeuroImage* 181 (November): 16–29.
- [Xu2017] Xu, Tiantian, Yuanjing Feng, Ye Wu, Qingrun Zeng, Jun Zhang, Jianzhong He, and Qichuan Zhuge. 2017. *A Novel Richardson-Lucy Model with Dictionary Basis and Spatial Regularization for Isolating Isotropic Signals*. *PloS One* 12 (1): e0168864.
- [Xu2014] Xu, Youyou, Yuanjing Feng, Yanpeng Niu, and Ye Wu. 2014. *ESTIMATION OF FIBER ORIENTATION DISTRIBUTION WITH NON-NEGATIVE CONSTRAINED HIGHER ORDER TENSOR DECONVOLUTION*. *Journal of Systems Science and Mathematical Sciences*. Xitong Kexue Yu Shuxue, 07.
- [Wu2015b] Ye, Wu, Feng Yuanjing, Li Fei, and Gao Chengfeng. 2015. *A Novel Fiber Orientation Distribution Reconstruction Method Based on Dictionary Basis Function Framework*. *Chinese Journal of Biomedical Engineering*, 03.
- [Yue2021] Yue, Ling, Dan Hu, Han Zhang, Junhao Wen, Ye Wu, Wei Li, Lin Sun, et al. 2021. *Prediction of 7-Year's Conversion from Subjective Cognitive Decline to Mild Cognitive Impairment*. *Human Brain Mapping* 42 (1): 192–203.
- [Yue2019] Yue, Ling, Dan Hu, Han Zhang, Junhao Wen, Ye Wu, Tao Wang, Dinggang Shen, and Shifu Xiao. 2019a. *Prediction of 7-Year Progression from Subjective Cognitive Decline to MCI*. In OHBM, Rome, Italy, June 9–13, 2019.
- [Zhang2019a] Zhang, Fan, Ye Wu, Isaiah Norton, and Lauren J. O'Donnell. 2019. *White Matter Parcellation Test-Retest Reproducibility of Diffusion MRI Tractography Fiber Clustering*. In Proceedings of the International Society of Magnetic Resonance in Medicine (ISMRM).
- [Zhang2019b] Zhang, Fan, Ye Wu, Isaiah Norton, Yogesh Rathi, Alexandra J. Golby, and Lauren J. O'Donnell. 2019. *Test-Retest Reproducibility of White Matter Parcellation Using Diffusion MRI Tractography Fiber Clustering*. *Human Brain Mapping* 40 (10): 3041–57.
- [Zhang2018a] Zhang, Fan, Ye Wu, Isaiah Norton, Yogesh Rathi, Nikos Makris, and Lauren J. O'Donnell. 2018. *A Data-Driven Groupwise Fiber Clustering Atlas for Consistent White Matter Parcellation and Anatomical Tract Identification of Subjects across the Lifespan*. In Annual Meeting of the International Society for Magnetic Resonance in Medicine (ISMRM).
- [Zhang2018b] Zhang, Fan, Ye Wu, Isaiah Norton, Laura Rigolo, Yogesh Rathi, Nikos Makris, and Lauren J. O'Donnell. 2018. *An Anatomically Curated Fiber Clustering White Matter Atlas for Consistent White Matter Tract Parcellation across the Lifespan*. *NeuroImage* 179 (October): 429–47.
- [Zhang2020a] Zhang, Huifeng, Lena Palaniyappan, Yan Wu, Enchao Cong, Chuangxin Wu, Lei Ding, Feng Jin, et al. 2020. *The Concurrent Disturbance of Dynamic Functional and Structural Brain Connectome in Major Depressive Disorder: The Prefronto-Insular Pathway*. *Journal of Affective Disorders* 274 (September): 1084–90.
- [Zhang2016] Zhang, Jun, Tiantian Xu, Yuanjing Feng, Ye Wu, Yongqiang Li, Jianzhong He, and Siqi Zhou. 2016. *A Self-Adaptive Local Feature Extraction Based Magnetic Resonance Imaging*. In 2016 Chinese Control and Decision Conference (CCDC), 6563–67. IEEE.
- [Founder] Ye Wu

*@ University of North Carolina at Chapel Hill*

[Director] Pew-Thian Yap

*@ University of North Carolina at Chapel Hill*

[Developer] Sahar Ahmad

*@ University of North Carolina at Chapel Hill*

[Developer] Yoonmi Hong

*@ University of North Carolina at Chapel Hill*

[Developer] Khoi Minh Huynh

*@ University of North Carolina at Chapel Hill*

[Contributor] Tiantian Xu

*@ Northwestern Polytechnical University*

[Contributor] Hoyt Patrick Taylor IV

*@ University of North Carolina at Chapel Hill*

[Contributor] Geng Chen

*@ Northwestern Polytechnical University*

[Contributor] Peng Sun

*@ Northwestern Polytechnical University*